



Magneto-Mechanical Response in Ni-Mn-Ga Magnetic Shape Memory Alloys

Leon M. Cheng

Rosaura Ham-Su

Shannon P. Farrell

Calvin V. Hyatt

Defence R&D Canada – Atlantic

Technical Memorandum

DRDC Atlantic TM 2004-267

December 2004

Report Documentation Page		Form Approved OMB No. 0704-0188
Public reporting burden for the collection of information is estimated to average 1 hour per response, including the time for reviewing instructions, searching existing data sources, gathering and maintaining the data needed, and completing and reviewing the collection of information. Send comments regarding this burden estimate or any other aspect of this collection of information, including suggestions for reducing this burden, to Washington Headquarters Services, Directorate for Information Operations and Reports, 1215 Jefferson Davis Highway, Suite 1204, Arlington VA 22202-4302. Respondents should be aware that notwithstanding any other provision of law, no person shall be subject to a penalty for failing to comply with a collection of information if it does not display a currently valid OMB control number.		
1. REPORT DATE DEC 2004	2. REPORT TYPE	3. DATES COVERED -
4. TITLE AND SUBTITLE Magneto-Mechanical Response in Ni-Mn-Ga Magnetic Shape Memory Alloys		5a. CONTRACT NUMBER
		5b. GRANT NUMBER
		5c. PROGRAM ELEMENT NUMBER
6. AUTHOR(S)	5d. PROJECT NUMBER	
	5e. TASK NUMBER	
	5f. WORK UNIT NUMBER	
7. PERFORMING ORGANIZATION NAME(S) AND ADDRESS(ES) Defence R&D Canada -Atlantic,PO Box 1012,Dartmouth, NS,CA,B2Y 3Z7		8. PERFORMING ORGANIZATION REPORT NUMBER
9. SPONSORING/MONITORING AGENCY NAME(S) AND ADDRESS(ES)		10. SPONSOR/MONITOR'S ACRONYM(S)
		11. SPONSOR/MONITOR'S REPORT NUMBER(S)
12. DISTRIBUTION/AVAILABILITY STATEMENT Approved for public release; distribution unlimited		
13. SUPPLEMENTARY NOTES The original document contains color images.		

14. ABSTRACT

It is generally accepted that the large reversible, magnetic-field-induced strain observed in ferromagnetic shape memory alloys is due to the rearrangement of twin variants in the martensite by an applied magnetic field leading to an overall change of shape. The main thermodynamic driving force for twin boundary motion in the presence of a magnetic field is the high magnetocrystalline anisotropy of the low-symmetry martensitic phase. Low twin boundary energy, high magnetocrystalline anisotropy energy and saturation magnetization are some of the key factors for large magnetic field induced strain. In order to achieve optimum performance, thermomechanical and magnetic treatments are necessary. In this investigation, a systematic investigation is being carried out on single crystals of Ni-Mn-Ga alloys to determine the combined effects of composition and thermomagneto-mechanical treatments on the crystal structure of the martensitic phases and the magnetomechanical properties of the Ni-Mn-Ga alloys. Repeated mechanical and magnetic forces have been applied to the samples. The results demonstrate that prior history has strong influence on the twinning start stress and twinning strain. In addition, heat treatment of the materials seems to increase the amount of strain that can be obtained (e.g. increased from 3% to 6%). Moreover, there is indication that prior heat treatment may also affect the martensite crystal structure that is formed during cooling. A systematic investigation has also been carried out to determine the effect of temperature on the magneto-mechanical behaviour of the Ni-Mn-Ga alloys. Strong temperature dependence of the magnetic shape memory effect in a Ni_{47.8}Mn_{27.5}Ga_{24.7} alloy has been observed. Twinning start and finish stresses, critical magnetic field and maximum magnetic-field-induced strain all remain almost constant within about 20°C below the martensite finish temperature and then change substantially at lower temperatures. Eventually no magnetic-field-induced strain can be observed at temperatures below -11°C. It is proposed that although magnetic anisotropy constant increases with decreasing temperature, it is not sufficient to overcome the increasing twinning stresses required for twin boundary motion at lower temperatures.

15. SUBJECT TERMS

16. SECURITY CLASSIFICATION OF:

a. REPORT

unclassified

b. ABSTRACT

unclassified

c. THIS PAGE

unclassified17. LIMITATION OF
ABSTRACT18. NUMBER
OF PAGES**44**19a. NAME OF
RESPONSIBLE PERSON

This page intentionally left blank.

Magneto-Mechanical Response in Ni-Mn-Ga Magnetic Shape Memory Alloys

Leon M. Cheng
Rosaura Ham-Su
Shannon P. Farrell
Calvin V. Hyatt

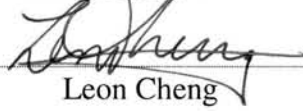
Defence R&D Canada – Atlantic

Technical Memorandum

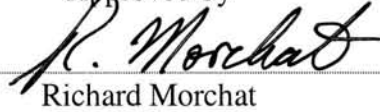
DRDC Atlantic TM 2004-267

December 2004

Author




Approved by



Richard Morchat

Section Head / Emerging Materials

Approved for release by



Kirk Foster

DRP Chair

© Her Majesty the Queen as represented by the Minister of National Defence, 2004

© Sa majesté la reine, représentée par le ministre de la Défense nationale, 2004

Abstract

It is generally accepted that the large reversible, magnetic-field-induced strain observed in ferromagnetic shape memory alloys is due to the rearrangement of twin variants in the martensite by an applied magnetic field leading to an overall change of shape. The main thermodynamic driving force for twin boundary motion in the presence of a magnetic field is the high magnetocrystalline anisotropy of the low-symmetry martensitic phase. Low twin boundary energy, high magnetocrystalline anisotropy energy and saturation magnetization are some of the key factors for large magnetic field induced strain. In order to achieve optimum performance, thermomechanical and magnetic treatments are necessary. In this investigation, a systematic investigation is being carried out on single crystals of Ni-Mn-Ga alloys to determine the combined effects of composition and thermo-magneto-mechanical treatments on the crystal structure of the martensitic phases and the magneto-mechanical properties of the Ni-Mn-Ga alloys. Repeated mechanical and magnetic forces have been applied to the samples. The results demonstrate that prior history has strong influence on the twinning start stress and twinning strain. In addition, heat treatment of the materials seems to increase the amount of strain that can be obtained (e.g. increased from 3% to 6%). Moreover, there is indication that prior heat treatment may also affect the martensite crystal structure that is formed during cooling. A systematic investigation has also been carried out to determine the effect of temperature on the magneto-mechanical behaviour of the Ni-Mn-Ga alloys. Strong temperature dependence of the magnetic shape memory effect in a $\text{Ni}_{47.8}\text{Mn}_{27.5}\text{Ga}_{24.7}$ alloy has been observed. Twinning start and finish stresses, critical magnetic field and maximum magnetic-field-induced strain all remain almost constant within about 20°C below the martensite finish temperature and then change substantially at lower temperatures. Eventually no magnetic-field-induced strain can be observed at temperatures below -11°C. It is proposed that although magnetic anisotropy constant increases with decreasing temperature, it is not sufficient to overcome the increasing twinning stresses required for twin boundary motion at lower temperatures.

Résumé

Il est généralement admis que l'importante déformation réversible induite par champ magnétique dans des alliages ferromagnétiques à mémoire de forme est due à un réarrangement de variantes de maillage dans la martensite. La principale force thermodynamique de mouvement limite (limitrophe, frontière) de maillage sous champ magnétique est la haute anisotropie magnétocristalline de la phase martensitique à faible symétrie. Une faible énergie de maillage limite, une haute énergie d'anisotropie magnétocristalline et une saturation de magnétisation sont parmi les principaux facteurs de déformation induite par haut champ magnétique. Pour favoriser un comportement optimal du matériau, des traitements thermomécaniques et magnétiques

sont nécessaires. Notre étude a procédé par observation systématique de cristaux simples d'alliages Ni-Mn-Ga soumis à diverses combinaisons de composition et de traitements thermo-magnéto-mécaniques. Elle avait pour but de déterminer l'effet de telles combinaisons sur la structure des cristaux de phases martensitiques, ainsi que les propriétés magnéto-mécaniques de ces alliages. Des forces mécaniques et magnétiques répétées ont été appliquées aux échantillons. Les tests ont démontré que l'historique de traitement du matériau influe grandement sur la tension d'amorce et sur la déformation de maillage. Un traitement thermique du matériau semble accroître la déformation pouvant en être obtenue (par exemple, de 3 %, à 6 %). Il semble aussi que le traitement thermique préalable du matériau affecte aussi la structure du cristal de martensite formé durant le refroidissement. Nous avons aussi étudié systématiquement l'effet de la température sur le comportement magnéto-mécanique des alliages Ni-Mn-Ga. Nous avons alors constaté une forte interdépendance entre la température et l'effet mémoire de forme magnétique d'un alliage $\text{Ni}_{47.8}\text{Mn}_{27.5}\text{Ga}_{24.7}$. Les tensions d'amorce et de fin de maillage, le champ magnétique critique et la déformation maximale induite par le champ magnétique restent tous pratiquement constants jusqu'à environ 20 °C sous la température de fin de martensite, mais ils varient considérablement à températures plus basses. De fait, plus aucune déformation induite par champ magnétique ne se produit à des températures inférieures à -11 °C. Nous en arrivons donc à conclure que même si la constante d'anisotropie magnétique augmente en fonction d'une température plus basse, cette constante n'est pas suffisante pour vaincre les tensions croissantes de maillage nécessaires pour forcer un mouvement limite de maillage à températures plus basses.

Executive summary

Introduction

Magnetic Shape Memory (MSM) alloys are a new class of actuator materials which produce strain by the reorientation of twin variants, in response to an applied magnetic field, and/or applied mechanical stress. So far, reversible strains of up to about 10% have been observed in Ni-Mn-Ga alloys. This is at least an order of magnitude larger than other magnetostrictive materials such as Terfenol-D (less than 0.2%). The unique combination of high strains, high actuation frequency (over 5kHz has been measured) and large energy densities make these materials promising for a variety of military and civilian applications. Potential applications include devices for vibration and signature control, energy harvesting, novel aerodynamic and hydrodynamic control systems, active shock amelioration systems and sonar devices.

Principal Results

The results from this investigation demonstrate that prior history has strong influence on the MSM effect of the Ni-Mn-Ga alloys. In one case, the induced strain increased from less than 1% to 4% due to repeated application of mechanical and magnetic forces. Moreover, strain increased from 4% to 6% in one case and from 8% to 14% in another case due to heat treatment. In order to achieve optimum performance of MSM alloys, thermomechanical and magnetic treatments are necessary. In addition, strong temperature dependence of MSM effect has been observed in a $\text{Ni}_{47.8}\text{Mn}_{27.5}\text{Ga}_{24.7}$ alloy. It has also been observed that twinning start and finish stresses, critical magnetic field and maximum magnetic-field-induced strain all remain almost constant within about 20°C below martensite finish temperature (31°C) and then change substantially at lower temperatures. Eventually no magnetic-field-induced strain can be observed at temperatures below -11°C.

Significance of Results

Results from this and related investigation demonstrate our capability in characterization of the magneto-mechanical properties of functional materials. The current results illustrate the importance of thermomechanical and magnetic treatments on the optimization of performance of MSM alloys. The observed strong temperature dependence of MSM effect illustrates a potential significant limitation on the application of these materials in some defence applications.

Future Work

Further study is being conducted to investigate whether similar strong temperature dependence can also be observed in Ni-Mn-Ga alloys with different compositions and structures, including commercially available Ni-Mn-Ga alloys.

Cheng, L.M., Ham-Su, R., Farrell, S.P., Hyatt, C.V. 2004. Magneto-Mechanical Response in Ni-Mn-Ga Magnetic Shape Memory Alloys. DRDC Atlantic TM 2004-267. Defence R&D Canada – Atlantic.

Sommaire

Introduction

Les alliages à mémoire magnétique de forme (AMF) constituent une nouvelle classe de matériaux actionneurs, grâce à leur capacité de se déformer par réorientation de variantes de maillage, sous l'effet d'un champ magnétique et/ou d'une contrainte mécanique. Jusqu'à présent, des déformations réversibles allant jusqu'à près de 10 % ont été observées dans des alliages de Ni-Mn-Ga. C'est là un ordre de grandeur bien supérieur à celui d'autres matériaux magnétostrictifs tels que le Terfenol-D (moins de 0,2 %). Leurs propriétés remarquables de déformation élevée, de haute fréquence d'activation (plus de 5 kHz, dans certains cas) et de grande densité énergétique les rendent aptes à diverses applications militaires et civiles, comme la mise au point de dispositifs de contrôle des vibrations et de signature, de collecte d'énergie, de contrôle aérodynamique et hydrodynamique, d'amortissement des secousses, et de dispositifs sonar.

Principaux résultats

Nos travaux ont démontré que l'historique de traitement du matériau influe grandement sur l'effet AMF d'alliages de Ni-Mn-Ga. Dans un cas, la déformation induite a augmenté de plus de 3 % (passant de moins de 1 % à 4 %) grâce à l'application répétée de forces mécaniques et magnétiques. L'ajout d'un traitement thermique a permis de faire passer le taux de déformation du matériau de 4 % à 6 % dans un cas, et de 8 % à 14 % dans un autre. Pour favoriser un comportement optimal des alliages AMF, des traitements thermomécaniques et magnétiques sont nécessaires. Nos travaux ont aussi démontré une forte interdépendance entre la température et l'effet mémoire de forme magnétique d'un alliage $\text{Ni}_{47,8}\text{Mn}_{27,5}\text{Ga}_{24,7}$. Ils ont démontré aussi que les tensions d'amorce et de fin de maillage, le champ magnétique critique et la déformation maximale induite par le champ magnétique restent tous pratiquement constants jusqu'à environ 20 °C sous la température de fin de martensite (31 °C), mais qu'ils varient considérablement à températures plus basses. De fait, plus aucune déformation induite par champ magnétique ne se produit à des températures inférieures à -11 °C.

Signification des résultats

Les résultats de cette étude et de travaux connexes démontrent notre capacité de caractériser les propriétés magnéto-mécaniques de matériaux fonctionnels, ainsi que l'importance de traitements thermomécaniques et magnétiques des alliages AMF pour en optimiser le comportement. Par contre, la forte interdépendance observée entre la température et l'effet AMF laisse entrevoir une limitation éventuelle considérable dans l'application de ces matériaux à des systèmes de défense.

Travaux futurs

Une étude complémentaire est nécessaire pour vérifier si une dépendance aussi grande à la température caractérise aussi les alliages de Ni-Mn-Ga de compositions et de structures diverses – y compris ceux disponibles sur le marché commercial.

Cheng, L.M., Ham-Su, R., Farrell, S.P., Hyatt, C.V. 2004. Réponse magnéto-mécanique d'alliages Ni-Mn-Ga à mémoire de forme magnétique. RDDC Atlantique TM 2004-267. R & D pour la défense Canada – Atlantique.

Table of contents

Abstract.....	i
Executive summary	iii
Sommaire.....	iv
Table of contents	v
List of figures	vii
Acknowledgements	ix
1. Introduction	1
1.1 Ni-Mn-Ga Alloys	1
1.2 Magneto-Mechanical Response.....	4
2. Experimental.....	6
3. Results and Discussion	10
3.1 Effects of Repeated Applications of Mechanical Forces.....	10
3.2 Effects of Temperature	19
4. Conclusions	23
5. References	24
Distribution list.....	26

This page intentionally left blank.

List of figures

Figure 1. Illustration of tetragonal variant structures and associated magnetizations.	2
Figure 2. Illustration of twinning as a mode of accommodation for internal strains induced by the martensite transformation. (a) Parent phase, (b) internal strain associated with pure lattice deformation and accommodation of internal strain through (c) twinning and (d) dislocation slip.	3
Figure 3. Motion of twin boundaries due to the application of a magnetic field or stress.	4
Figure 4. Differential scanning calorimetry curve for a sample from bottom of boule # 23.	7
Figure 5. Experimental apparatus used to measure magneto-mechanical response at various temperatures.	9
Figure 6. Stress–strain curves for three subsequent compression tests on sample 25-1-14: (a) compression along long axis; (b) compression along one of the short axis and (c) compression along the other short axis.	10
Figure 7. Stress–strain curves for a series of compression tests on sample 27-8-1-13. After each test, the sample was rotated 90° such that compressive load could then be applied along the axis with the largest increase in length: (a) 1st; (b) 2nd (c) 4th and (d) 7th compression.	12
Figure 8. M–H curves of sample 27-8-1-13 with the magnetic field applied along the different directions as indicated.	12
Figure 9. Stress–strain curves for a series of compression tests on sample 25-1-9. Compression load was applied to the 4 mm and 5 mm axes alternatively: (a) 1st compression; (b) 2nd compression (c) 3rd compression and (d) 10th compression.	13
Figure 10. Stress–strain curves for a series of compression tests on sample 25-1-9 after heat treatment. Compression load was applied to the 4mm and 5mm axes alternatively: (a) 1st compression and (b) 5th compression.	14
Figure 11. M–H curves of sample 25-1-9 with the magnetic field applied along the different directions as indicated: (a) before; and (b) after thermo-magneto treatment, respectively.	14
Figure 12. Stress–strain curves for a series of compression tests on sample 25-1-12 after heat treatment. (a) 1st compression along the 6 mm axis, (b) 2nd compression along the 3 mm axis, (c) 3rd compression along the 2.5 mm axis and (d) 4th compression along the 6 mm axis.	15
Figure 13. Stress–strain curves for a series of compression tests on sample 25-1-12 after applying magnetic field. (a) 1st compression along the 3 mm axis, (b) 2nd compression	

along the 6 mm axis, (c) 3rd compression along the 2.5 mm axis and (d) 4th compression along the 6 mm axis.	16
Figure 14. Differential Scanning Calorimeter curves for (a) sample 25-1-12 and (b) a small piece from sample 25-1-12 after compression tests.	17
Figure 15. Stress–strain curves for a series of compression tests on sample 25-1-12 after DSC analysis: (a) 1st compression and (b) 3rd compression.	18
Figure 16. (a) Stress–strain curves and (b) twinning start stress of sample 25-1-15 during uniaxial compression as a function of temperature.	20
Figure 17. Effect of temperature on magnetic-field-induced strain in sample 25-1-15.....	21
Figure 18. (a) Critical magnetic field and (b) maximum magnetic-field-induced strain as a function of temperature.	21

List of tables

Table 1. Chemical compositions of samples (atomic %)	6
Table 2. Martensite (M_S , M_F) and Austenite (A_S , A_F) start and finish transformation temperatures and Curie temperatures (T_C) of samples.	7

Acknowledgements

Special thanks to Mr. Bob Armstrong, Mr. Irv Keough and Mr. Gary Fisher of DRDC Atlantic for their technical assistance. The authors would also like to thank Dr. Jian Chen of Dalhousie University, Dr. Michael Gharghouri of NRC and Professor Craig Bennett of Acadia University. Their ideas and fruitful discussions contributed significantly to this work.

This page intentionally left blank.

1. Introduction

Magnetic shape memory (MSM) alloys are a new class of smart materials that exhibit large reversible strains when exposed to a magnetic field. These materials have received much attention in recent years since Ullakko *et al.* [1] observed a large reversible, magnetic-field-induced strain in Ni-Mn-Ga alloys. So far, reversible magnetic-field-induced strains of up to about 10% [2,3] have been observed in off-stoichiometric Ni-Mn-Ga alloys. This is at least an order of magnitude larger than other magnetostrictive materials such as Terfenol-D (less than 0.2%). Although strains offered by magnetic shape memory alloys are similar in magnitude to conventional shape memory alloys, the faster response due to magnetic control makes them more promising for a variety of applications. Potential applications include devices for vibration and signature control, energy harvesting, novel aerodynamic and hydrodynamic control systems, active shock amelioration systems and sonar devices.

Unlike the conventional, temperature-driven shape memory effect in which the reversible strain is related to the diffusionless structural phase transformation from a high-temperature high-symmetry phase to a low-temperature low-symmetry martensitic phase; it is generally accepted that the magnetic shape memory effect is due to the rearrangement of twin variants in the martensite by an applied magnetic field leading to an overall change of shape [1-9].

So far, MSM effect has been found to be most significant in Ni-Mn-Ga alloys and these materials are the most extensively studied. However, Ni-Mn-Ga alloys continue to evolve and as such, the full potential of these materials has yet to be realized. Substantial efforts have been directed at understanding the phenomenology and determining the magneto-mechanical properties of Ni-Mn-Ga alloys.

1.1 Ni-Mn-Ga Alloys

Off-stoichiometric Ni-Mn-Ga alloys are capable of significant dimensional changes when a magnetic field, stress or thermal energy is applied. These dimensional changes are directly related to the change in the crystal structure or crystallographic orientation of the material. The structural and magnetic transformations of Ni-Mn-Ga alloys are complex, and depend on composition (including quaternary additions) and thermal, magnetic and stress history. At high temperature, the austenitic parent phase is paramagnetic and has a cubic Huesler ($L2_1$) type crystal structure [10]. These alloys undergo a paramagnetic-ferromagnetic transformation of the $L2_1$ cubic phase at the Curie temperature, and a structural transformation of the cubic parent structure to several possible lower-symmetry martensite structures. When cooled below a critical temperature, called the martensite start temperature (M_s), martensite with a lower symmetry structure is formed through a combination of contraction, elongation and shearing of the lattice with no change in composition. The change in crystal structure is complete when the material is cooled to the martensite finish temperature (M_f). The dimensional change incurred when the cubic austenite phase transforms to a few of the

several lower symmetry variants in the martensitic phase is illustrated in Figure 1. The reverse transformation occurs when the lower symmetry phase is heated above a critical temperature identified as the austenite start temperature (A_S). The material is completely transformed to the cubic austenite phase when heated to the austenite finish temperature (A_F). Above M_S and below a critical limiting temperature M_d , the martensitic transformation can also be triggered by the application of a stress.

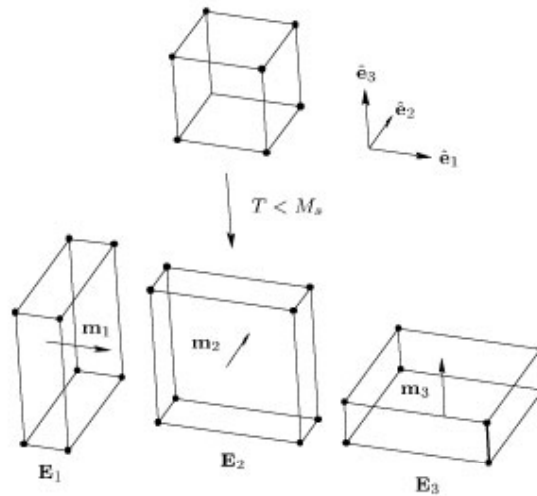


Figure 1. Illustration of tetragonal variant structures and associated magnetizations.

A significant internal strain is associated with the martensitic transformation due to the change in crystal structure. The net distortions can be accommodated by dislocation slip or twinning. For off-stoichiometric Ni-Mn-Ga alloys, the method of accommodation that has the lowest energy (therefore preferred) is usually twinning, as illustrated in Figure 2. In this case, twin variants with different contraction axes will be formed to reduce the internal strain.

The magnetic shape memory effect in these alloys is related to the rearrangement of twin variants by an applied magnetic field leading to an overall change of shape. Martensite structure of off-stoichiometric Ni-Mn-Ga typically shows a strong magnetocrystalline anisotropy. The local crystallographic structure controls the easy axis of magnetization, so that each variant has a different direction for the easy axis of magnetization; this corresponds to the shortest axis in the crystallographic structure. If the anisotropy is sufficiently large, when an external magnetic field (below the saturation limit) is applied, it will be energetically favourable to redistribute the variants through the motion of twin boundaries such that the easy axis align with the magnetic field, rather than rotating the magnetizations with respect to their local crystal structure [11]. As a result, large dimension change can be observed in these alloys under an applied field. Figure 3 illustrates schematically how a system with two

variants would react to an applied magnetic field. The red and blue arrows in Figure 3 denote the easy axes of magnetization for two different twin variants, respectively. Application of the magnetic field induces the movement of twin boundaries so that favourably oriented variants occupy a larger volume fraction of the material. Since the easy axis of magnetization is along the short $\langle 100 \rangle$ axis of each variant, a compressive stress applied along the same axis will also favour the same variant. Applying a magnetic field or a compressive stress in an orthogonal direction can reverse twin boundary motion and return the material to its original geometry, assuming no other plastic deformation has occurred.

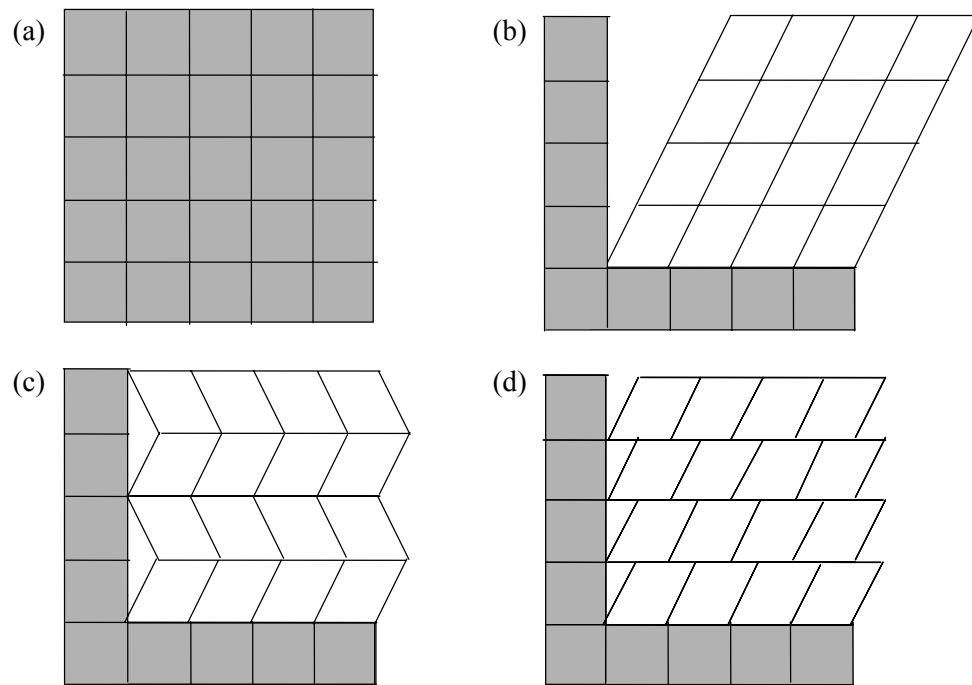


Figure 2. Illustration of twinning as a mode of accommodation for internal strains induced by the martensite transformation. (a) Parent phase, (b) internal strain associated with pure lattice deformation and accommodation of internal strain through (c) twinning and (d) dislocation slip.

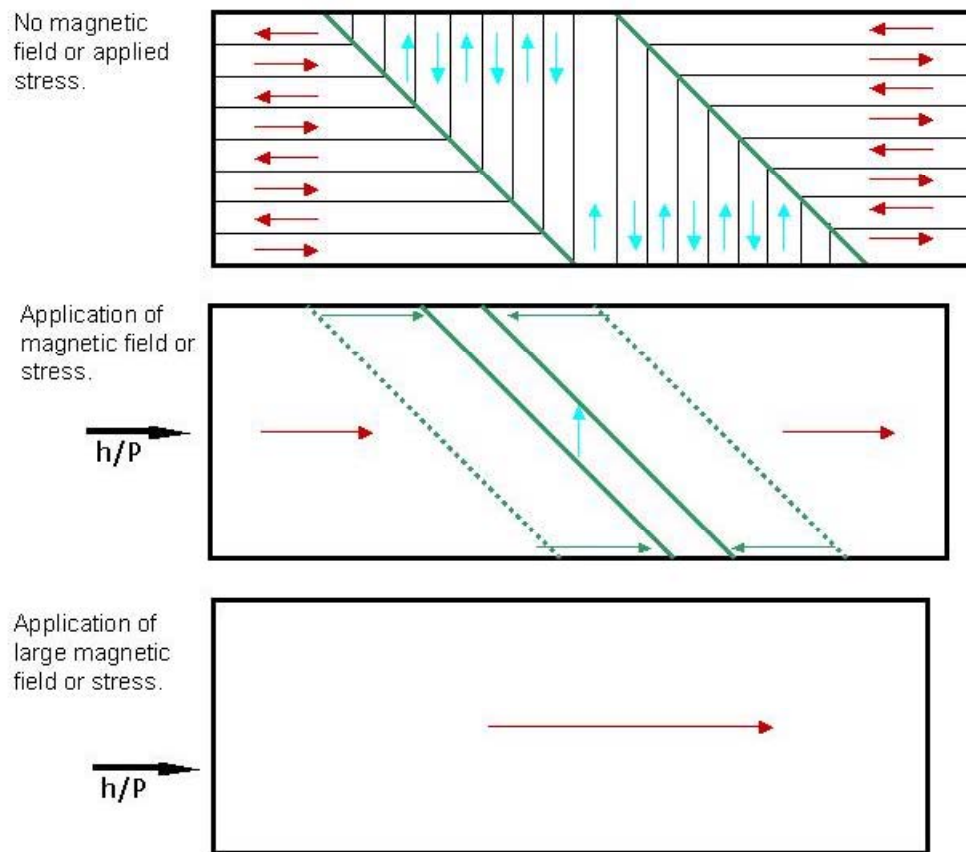


Figure 3. Motion of twin boundaries due to the application of a magnetic field or stress.

1.2 Magneto-Mechanical Response

The main thermodynamic driving force for twin boundary motion in the presence of a magnetic field is the high magneto-crystalline anisotropy of the low-symmetry martensitic phase. Low twin boundary energy, high magneto-crystalline anisotropy energy and saturation magnetization are some of the key factors for large magnetic field induced strain. Reversible magnetic-field-induced strains of up to 6% have been observed in Ni-Mn-Ga alloys with a tetragonal five-layered (5M) martensitic crystal structure [6-9]. Depending on the composition of the alloy and temperature, orthorhombic seven-layered (7M) and tetragonal non-layered (T) martensitic crystal structures have also been observed. In the Ni-Mn-Ga alloys with a 7M orthorhombic martensite, up to 10% magnetic-field-induced strains [2,3] have been observed. However, even though up to about 20% stress-induced strain has been reported in the non-layered tetragonal martensite, so far no magnetic-field-induced strain has been observed in this structure [12,13].

The reported measurements on the MSM effect and the magneto-mechanical properties in single crystals of Ni-Mn-Ga alloys can vary significantly due to their strong dependence on crystal structure, composition, initial microstructure and the volume fraction of the different variants [3,5,14,15]. One of the purposes of the current work is to investigate the combined effects of composition and thermomechanical treatments on the crystal structure of the martensitic phases and the magneto-mechanical properties of the Ni-Mn-Ga alloys. In addition, a systematic investigation is being carried out on single crystals of Ni-Mn-Ga alloy to determine the effect of temperature on the magneto-mechanical behaviour of the Ni-Mn-Ga alloys. Repeated mechanical and magnetic forces have been applied at various temperatures below the martensite finish (M_F) temperature. The magnetization of single crystals of Ni-Mn-Ga was measured as a function of magnetic field using a vibrating sample magnetometer (VSM). The dependence of martensitic transformation characteristics on composition and prior thermomechanical treatments was also investigated by differential scanning calorimetry (DSC).

The remainder of this document is structured as follows: A description of the experimental methods used in this work is presented in section 2. Experimental results are presented in section 3, along with a discussion of their significance; followed by conclusions derived from this work in Section 4.

2. Experimental

Ni-Mn-Ga samples used in this investigation were prepared by directional solidification using a seedless Bridgman crystal growth method. The alloys were grown in a high purity alumina crucible that was pulled through a temperature gradient at a growth rate of 2.8 mm/hr in an argon atmosphere. During the directional solidification, temperature was monitored with an optical pyrometer and the melt temperature was held between 1350°C and 1420°C. Details of the method were published elsewhere [16].

Compositional analysis was performed by either inductively coupled plasma–atomic emission spectroscopy (ICP-AES) on samples dissolved in nitric acid or by scanning electron microscopy coupled with energy dispersive spectroscopy (SEM-EDS). Chemical analysis results have the following accuracies: Ni: $\pm 0.6\%$, Mn: $\pm 0.4\%$, and Ga: $\pm 0.3\%$ at the 95% confidence intervals. Macro-segregation was found along the longitudinal axis of the boules (growing direction). Samples were taken from various locations along the length of the boules to obtain different compositions. Compositions in atomic percentage for the samples are shown in Table 1.

Table 1. Chemical compositions of samples (atomic %)

Sample ID	Boule #	Ni (at%)	Mn (at%)	Ga (at%)
25-1-9	25, bottom	52.9	27.3	19.8
25-1-12	25, top	48.8	30.2	21.0
25-1-14	25, top	48.1	31.5	20.4
27-8-1-13	27, top	48.6	31.5	19.9
25-1-15*	25, middle	47.8	27.5	24.7

* Compositions of this sample were determined by SEM-EDS, all others determined by ICP-AES.

Martensite and austenite start and finish transformation temperatures for the tested samples were determined by using either a DSC 2910 differential scanning calorimeter manufactured by TA Instruments or a DSC 600 microscopic stage manufactured by Linkam Scientific Instruments. DSC analysis was carried out in an aluminum pan using a heating/cooling rate of 10°C/min and ultra high purity nitrogen purge gas at a flow rate of 25 ml/min. A NIST indium melting point standard was used as the calibration standard. The effect of up to four heating/cooling cycles was investigated with this technique. For most samples, DSC cycling consisted of controlled heating from -50°C to 150°C and controlled cooling to -10°C, followed by as many cycles of reheating to 150°C and cooling to -10°C as required. A typical DSC curve for a Ni-

Mn-Ga sample is shown in Figure 4. Curie temperatures were determined using a TA Instruments thermo-gravimetric analyser (TGA); modified for Curie temperature determination with the addition of a magnet below the weighing pan. The transformation temperatures and Curie temperatures for the samples are shown in Table 2. It is apparent that both the martensitic and austenitic phases are ferromagnetic over the temperature range studied.

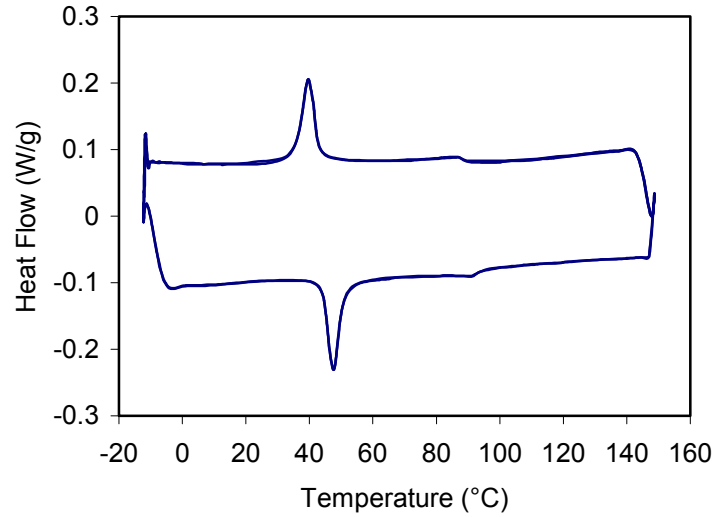


Figure 4. Differential scanning calorimetry curve for a sample from bottom of boule # 23.

Table 2. Martensite (M_S , M_F) and Austenite (A_S , A_F) start and finish transformation temperatures and Curie temperatures (T_C) of samples.

Sample ID	M_S (°C)	M_F (°C)	A_S (°C)	A_F (°C)	T_C (°C)
25-1-9	30	24	35	40	93
25-1-12	40	34	41	50	93
25-1-14	47	37	46	56	89
27-8-1-13	45	35	45	55	88
25-1-15	31	40	50	58	93

Single crystals, approximately 6 mm in diameter and 60 mm in length were isolated from the as-cast boules. One end of each crystal was cut and polished to 1 μm for orientation purposes. Orientations of single crystals in each boule were determined by Laue back-reflection x-ray diffraction using a Philips x-ray generator. A Tungsten tube provided the x-ray source and the generator operated at 20-25 kV and 10-25 Amps; these conditions were often varied to assist with indexing Laue patterns. The specimens were heated above the austenite finish temperature to ensure complete transformation to the austenite phase. This high temperature phase has the $L2_1$ cubic structure and has nearly the same crystallographic orientation as the martensite phase and is much easier to orient due to the higher symmetry and the absence of twins. In fact, the $(100)_M$, $(010)_M$ and $(001)_M$ planes of the body-center martensite structures are nearly parallel to the (100) , (010) and (001) planes of the parent cubic phase, and therefore one could reasonably apply a pseudo-cubic coordinate system to the different variants.

Single-crystal samples with dimensions range from 2mm \times 3mm \times 5mm to 3mm \times 3mm \times 7mm were machined using an electrical discharge machining (EDM) device. The faces of the prismatic single-crystal samples were nearly parallel to the (100) , (010) and (001) planes of the high temperature cubic phase. The parallelism of the end faces of the samples was ensured by a careful mechanical polish using a set of special polishing jigs [17].

Magnetization versus magnetic field (M-H) measurements were made at room temperature (23°C) using a Princeton Applied Research Model 155 vibrating sample magnetometer (VSM) with a maximum applied field restricted to 0.8 Tesla [18]. This field was measured using a calibrated Hall probe and the magnetization was calibrated using a high purity polycrystalline nickel rod and a single crystal of Yttrium Iron Garnet. The specimens were mounted between the pick-up coils and could be easily rotated for different field orientations. The room temperature measurements were sufficient to ensure that the specimens were both in the martensitic phase and ferromagnetic. For collection of magnetization curves of single-variant martensite, the twin boundaries must be constrained with an adhesive to prevent magnetic-field-induced redistribution of martensite variants during measurement. Data were determined for nearly single-variant oriented single crystals of martensite and austenite from magnetization curves collected along the $[100]$, $[010]$ and $[001]$ directions, of the parent structure, as a function of applied field.

Heat treatments were carried out on some samples prior to magnetic or magneto-mechanical measurements. For heat treatment, machined samples were first encapsulated in evacuated quartz. After annealing for 24 hours at 800°C in a 3-zone tube furnace, the samples were then immediately transferred to the 500°C zone in the same furnace and annealed for 24 hours at this temperature, followed by cooling in air to room temperature.

The mechanical tests were conducted using an Instron servohydraulic system with an Instron 8800 controller. Uniaxial compressions were applied at room temperature at a nominal strain rate of approximately $2 \times 10^{-3} \text{ s}^{-1}$. Due to the size of the sample, axial deformation was measured using the displacement of the crosshead. Dimensions of

each sample were measured before and after each test. Temperature dependence of magneto-mechanical response and magnetic-field-induced strain were characterized using an experimental apparatus [19] capable of applying longitudinal stress and transverse magnetic field simultaneously at various temperatures (Figure 5). Uniaxial compression experiments under orthogonal magnetic field were conducted on a single crystal sample at various temperatures ranging from -17°C to 23°C . Displacement along the compression direction was measured using a linear variable differential transducer (LVDT). In addition, dimensions of the sample were measured before and after each test.

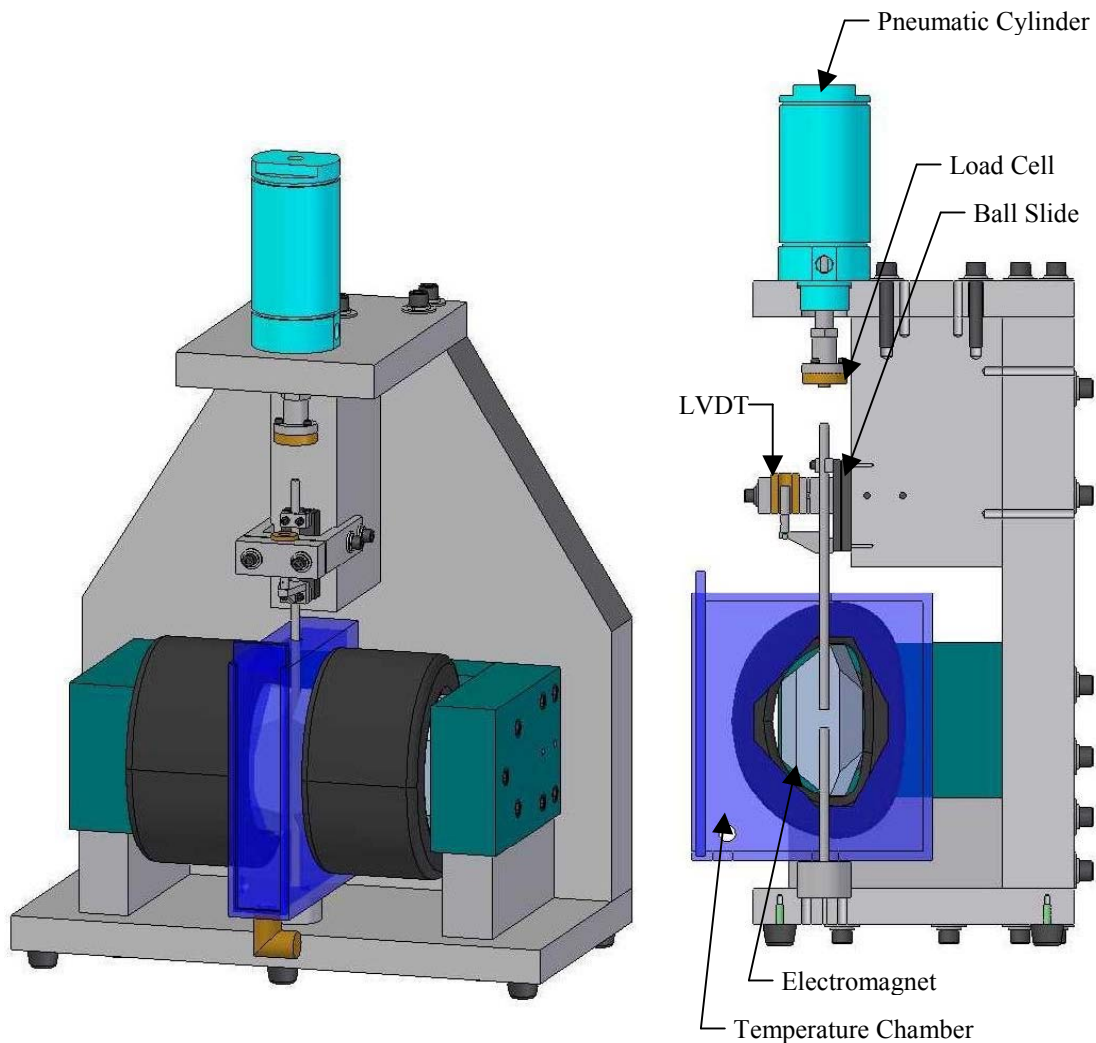


Figure 5. Experimental apparatus used to measure magneto-mechanical response at various temperatures.

3. Results and Discussion

3.1 Effects of Repeated Applications of Mechanical Forces

Figure 6a shows the stress-strain curve of oriented sample 25-1-14 under uniaxial compression. The rectangular sample was about 3mm×3mm×7mm with all the surfaces parallel to the {100} planes of the high temperature austenite phase. The uniaxial compression load was applied along the 7mm axis. The pseudo-elastic behaviour started at a stress level of about 44 MPa. The amount of strain induced by twin variants reorientation was about 1% and the reorientation completed at a stress level of about 65 MPa. After this compression, both of the two short axes increased in length.

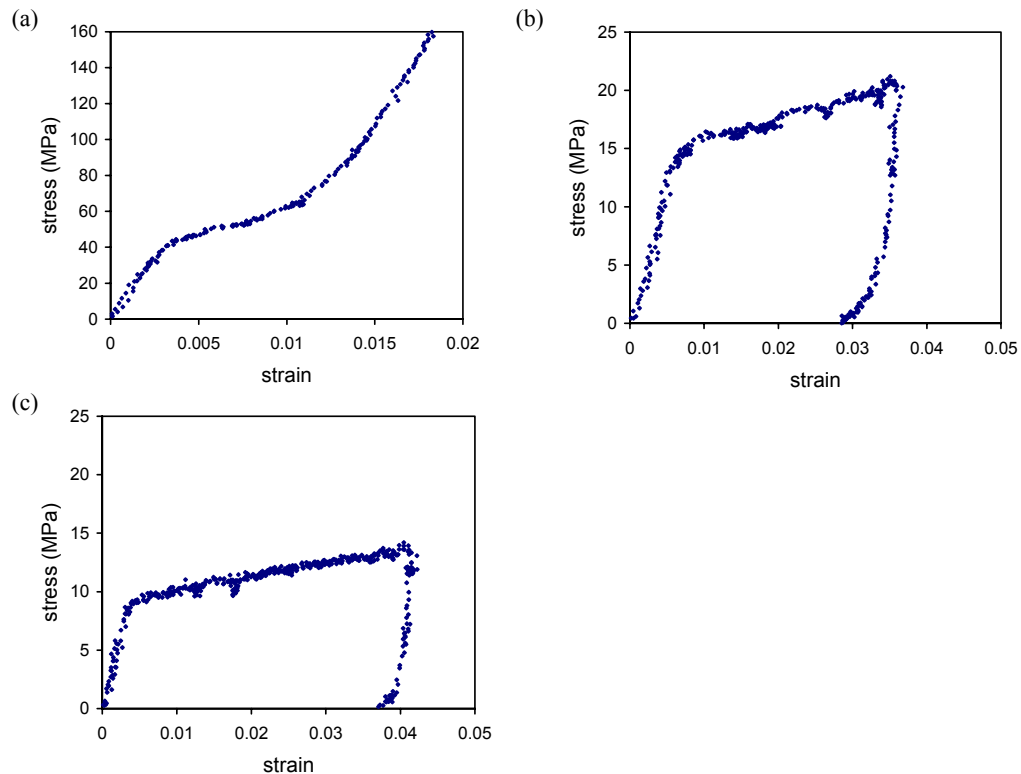


Figure 6. Stress–strain curves for three subsequent compression tests on sample 25-1-14: (a) compression along long axis; (b) compression along one of the short axis and (c) compression along the other short axis.

The sample was then rotated 90° and a compressive load was applied along one of the short axes (Figure 6b). As shown in Figure 6b, the starting stress for twin variants reorientation decreased to about 15 MPa. However, the test was programmed to unload before the twin variants reorientation completed. Therefore, the stress level to complete the reorientation was not determined. Nevertheless, the strain induced by twin variants reorientation was more than 3%, compared to 1% during the first compression. After the second compression, the other short axis increased in length but the length of the long axis remained almost the same. The sample was then rotated 90° again such that a compressive load could be applied along the short axis that increased in length. Figure 6c shows the stress-strain curve for this test. The starting stress for twin variants reorientation further decreased to about 9 MPa. As in the previous case, the test started to unload before the reorientation completed, therefore, the completing stress was not determined. Nevertheless, the amount of strain induced by twin variants reorientation increased to about 4%.

Before these tests, no special treatment was applied to the sample; therefore, it is likely that the sample had multiple twin variants initially. That may explain the high starting stress and small twinning strain from the first compression. However, after the first compression, the volume fraction of the variant with the easy axis parallel to the compression direction should increase due to the reorientation of twin variants. Thus, the strain that can be obtained from twin variants reorientation increased during the subsequent compressions.

Compression tests have also been conducted on sample 27-8-1-13, which has a composition similar to that of sample 25-1-14 (see Table 1). The rectangular sample was about 2mm×3mm×5mm in dimension. Figure 7 shows the stress-strain curves from a series of compression tests. After each test, the sample was rotated 90° such that compressive load could then be applied along the axis with the largest increase in length. The twinning start stress and complete stress were about 15 MPa and 35 MPa, respectively, for the 1st compression, while the strain was about 5%. However, during the 2nd compression, the twinning start and complete stresses decreased to about 8 MPa and 25 MPa, respectively, and the strain increased to about 8%. Even though the strain remained at about 8% for the subsequent compression, the twinning start and complete stresses gradually decreased to about 6 MPa and 22 MPa, respectively. After the 7th compression, a magnetic field of up to 0.9 T was applied to the sample along the axis that increased in length. However, no measurable change in dimensions could be detected. A magnetic field of up to 0.9 T was then applied along the other two axes in sequence; no measurable dimension change was detected in either case.

Magnetization vs magnetic field (M-H) curves for sample 27-8-1-13 are shown in Figure 8, with the field applied along the $[100]_M$, $[010]_M$ and $[001]_M$ directions of the crystal structure. These curves show the characteristic easy, intermediate and hard axis of magnetization typical of a single variant of orthorhombic 7M martensite. The magnetization has reached saturation near 52 emu/g along the $[001]$ direction of the sample, the easy axis of magnetization. The limitations of the magnet prevent the sample from reaching saturation when the field is applied along the other two axes. In addition, the lack of linearity for the M-H curve along the $[100]$ direction implies that this sample is not completely transformed to a single variant.

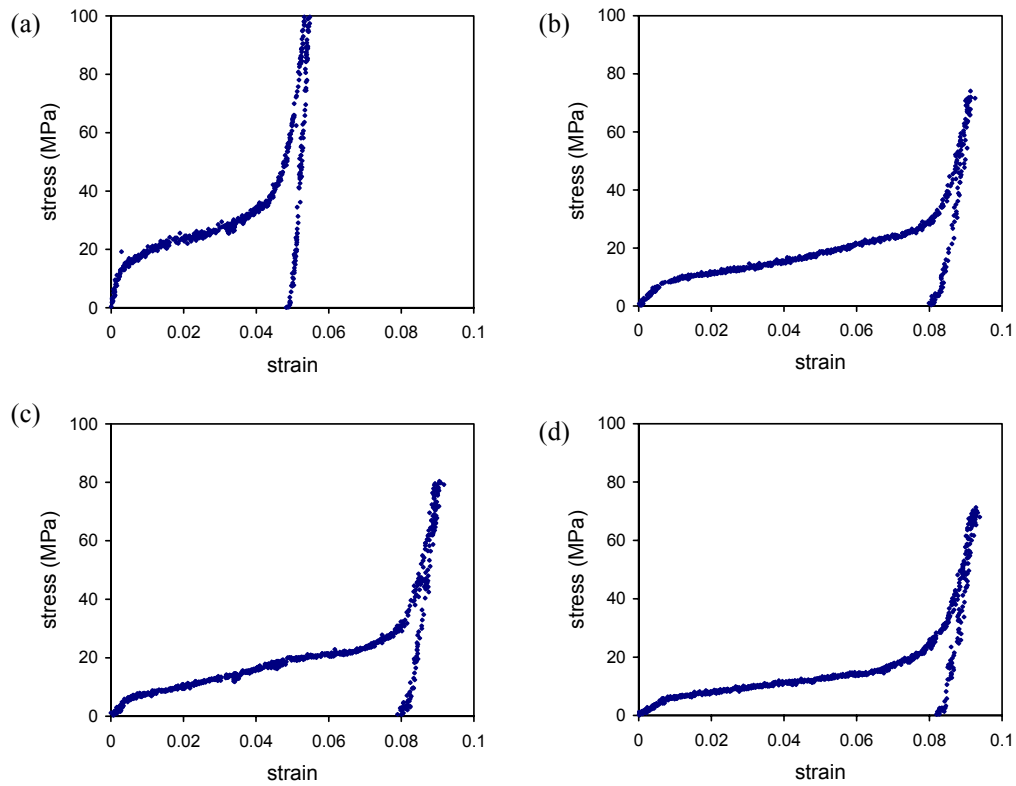


Figure 7. Stress–strain curves for a series of compression tests on sample 27-8-1-13. After each test, the sample was rotated 90° such that compressive load could then be applied along the axis with the largest increase in length: (a) 1st; (b) 2nd (c) 4th and (d) 7th compression.

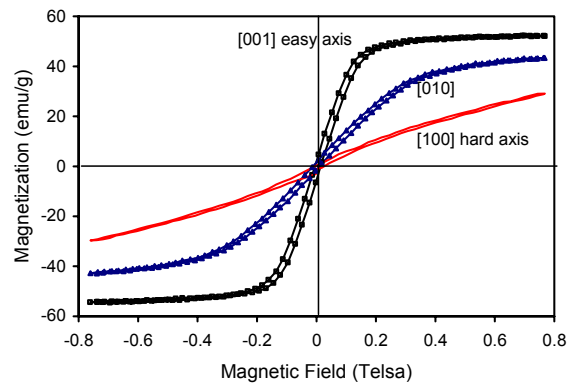


Figure 8. M – H curves of sample 27-8-1-13 with the magnetic field applied along the different directions as indicated.

Figure 9 shows the stress-strain curves from a series of compression tests conducted on sample 25-1-9. The rectangular sample was about 4mm×4mm×5mm in dimension. Compressive load was first applied to one of the 4 mm axes (Figure 9a). The twinning start stress was less than 4 MPa, but the strain was only about 1%. After the compression, the sample was rotated 90° and a compressive load was applied along the 5mm axis. Subsequent compression tests were then conducted with compressive load applied along these two axes alternatively. During the compression tests, there was almost no change in the length of the third axis. As shown in Figure 9b, the starting stress decreased to about 2 MPa during the 2nd compression while the strain increased to about 3.5%. During the subsequent compressions, the starting stress further decreased to less than 2 MPa with no significant changes in amount of twinning strain (Figures 9c and 9d). After the 10th compression, a magnetic field of up to 0.9 T was applied to the axis normal to the compression direction. A 2.2% magnetic-field-induced strain was detected.

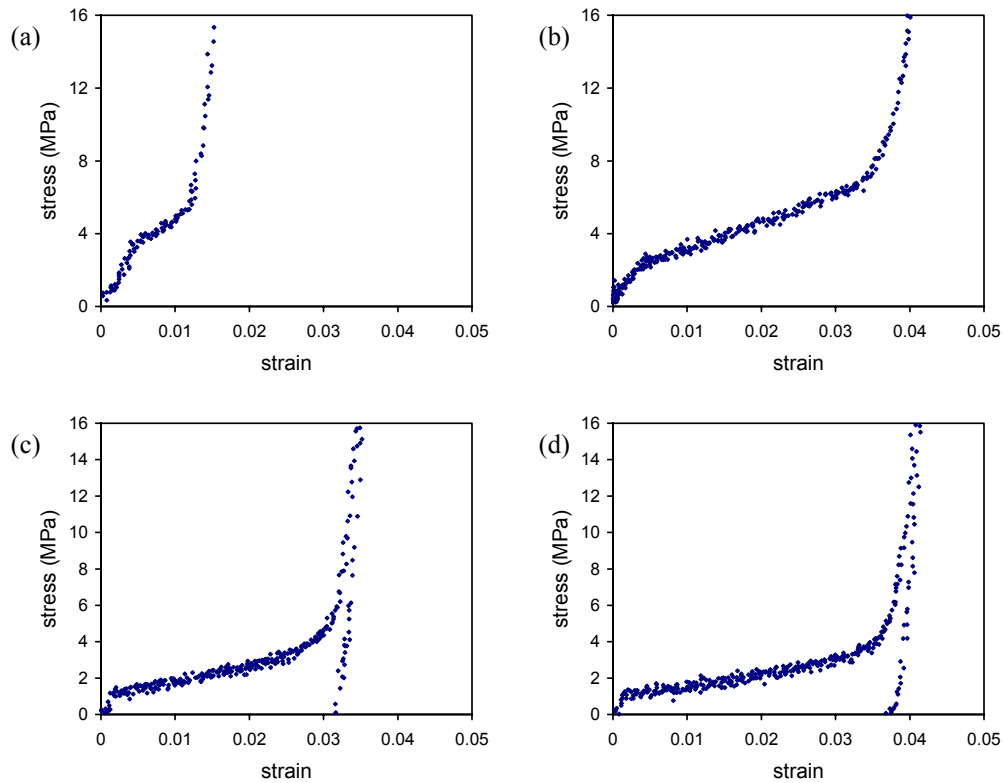


Figure 9. Stress–strain curves for a series of compression tests on sample 25-1-9. Compression load was applied to the 4 mm and 5 mm axes alternatively: (a) 1st compression; (b) 2nd compression (c) 3rd compression and (d) 10th compression.

The sample was then annealed for 24 hours at 800°C, followed by 24 hours at 500°C and then air-cooled. A series of compression tests were then conducted on the sample. The stress-strain curves are shown in Figure 10. There were no significant changes in twinning start stress after heat treatment, however, the amount of strain that could be obtained from stress-induced twin variants reorientation increased to about 6%. After the last compression, a magnetic field of up to 0.9 T was applied to the axis normal to the last compression direction. A 5.3% magnetic-field-induced strain was detected, compared to a 2.2% magnetic-field-induced strain before heat treatment.

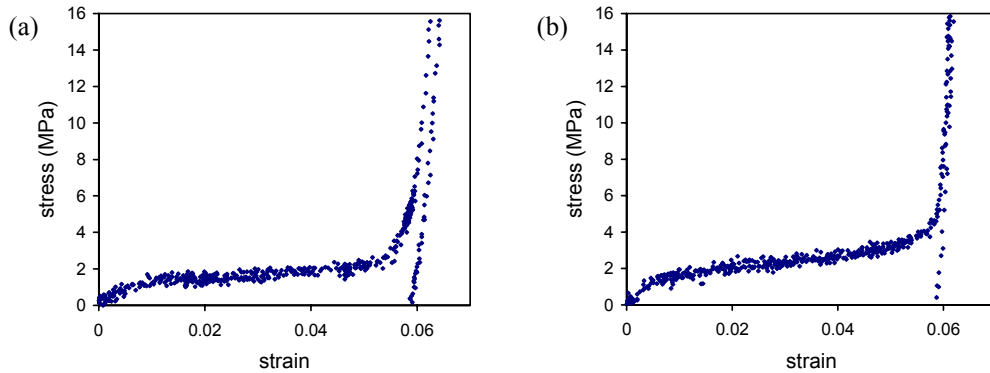


Figure 10. Stress–strain curves for a series of compression tests on sample 25-1-9 after heat treatment. Compression load was applied to the 4mm and 5mm axes alternatively: (a) 1st compression and (b) 5th compression.

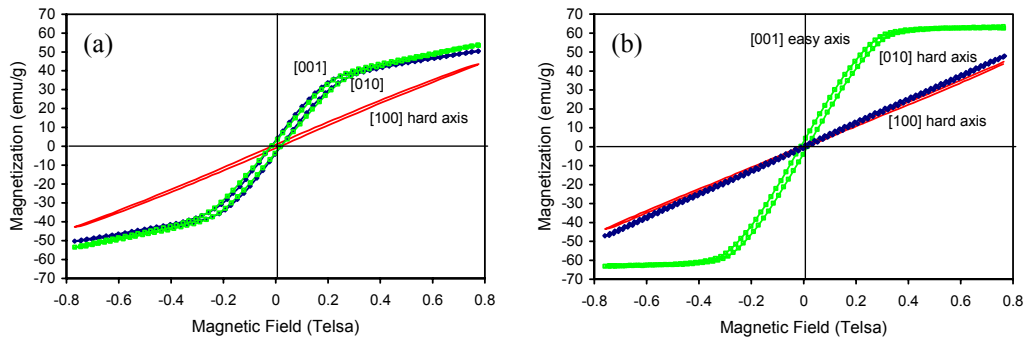


Figure 11. *M–H* curves of sample 25-1-9 with the magnetic field applied along the different directions as indicated: (a) before; and (b) after thermo-magneto treatment, respectively.

The M-H curves of sample 25-1-9 after heat treatment are shown in Figure 11a. The curves for the [001] and the [010] axes approach saturation initially with a slope consistent with the easy magnetization axis (see Figure 11b) and the subsequent slope is finite but between that of easy and hard axes. This characteristic of the curves suggests that the sample was in a state of mixture of two or more twin variants. Figure 11b shows the M-H curves of sample 25-1-9 after it was heated to above the Curie temperature and then subsequent cooling with a magnetic field of 0.9 T applied along the [001] axis direction. The shape of the M-H curves is typical of a single variant of tetragonal 5M martensite [20]. The strength of the uniaxial magnetic anisotropy constant is calculated to be $K_u = 1.8 \times 10^5 \text{ J/m}^3$, which is consistent with literature estimates for the tetragonal 5M martensite [7,14].

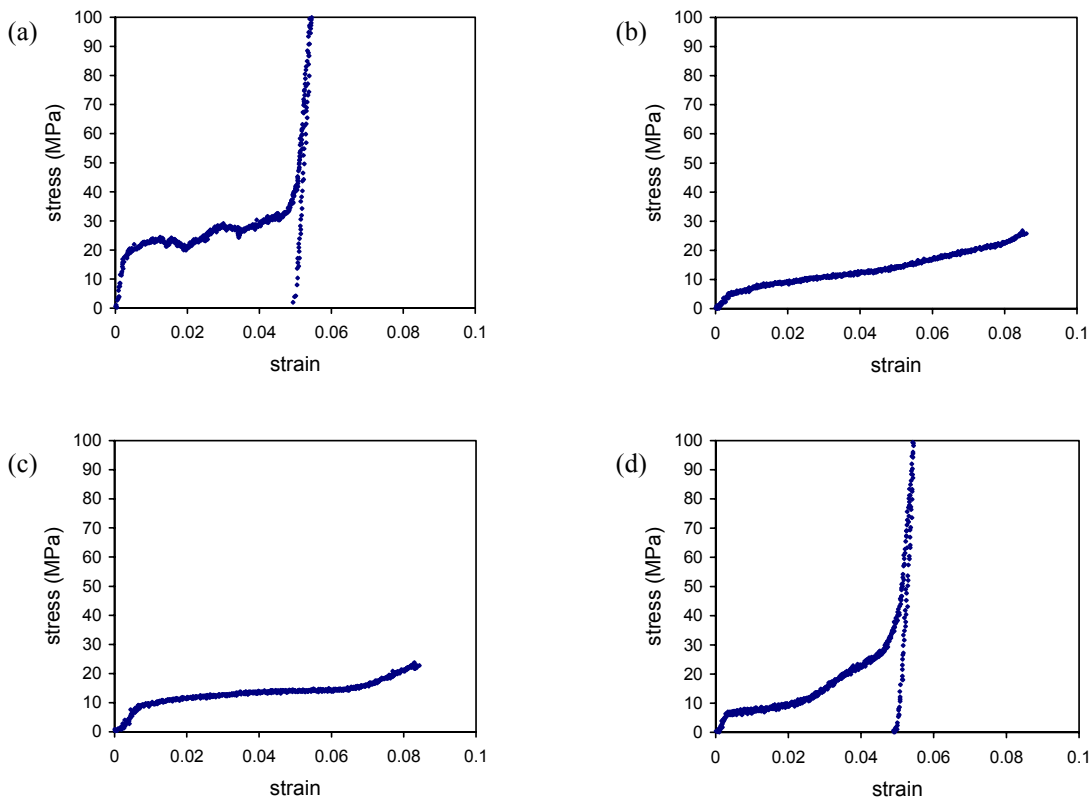


Figure 12. Stress–strain curves for a series of compression tests on sample 25-1-12 after heat treatment. (a) 1st compression along the 6 mm axis, (b) 2nd compression along the 3 mm axis, (c) 3rd compression along the 2.5 mm axis and (d) 4th compression along the 6 mm axis.

Stress-strain curves for a series of compression on sample 25-1-12 are shown in Figure 12. The rectangular sample was about 2.5mm×3mm×6mm in dimension. This sample and sample 25-1-14 were cut from the same crystal and were adjacent to each other near the top of the boule. Sample 25-1-12 was annealed at 800°C for 24 hours, followed by 24 hours at 500°C and then air-cooled. The composition of this sample (Table 1) is slightly different from that of sample 25-1-14. This may be due to segregation during crystal growth and loss of Mn during crystal growth and the subsequent heat treatment.

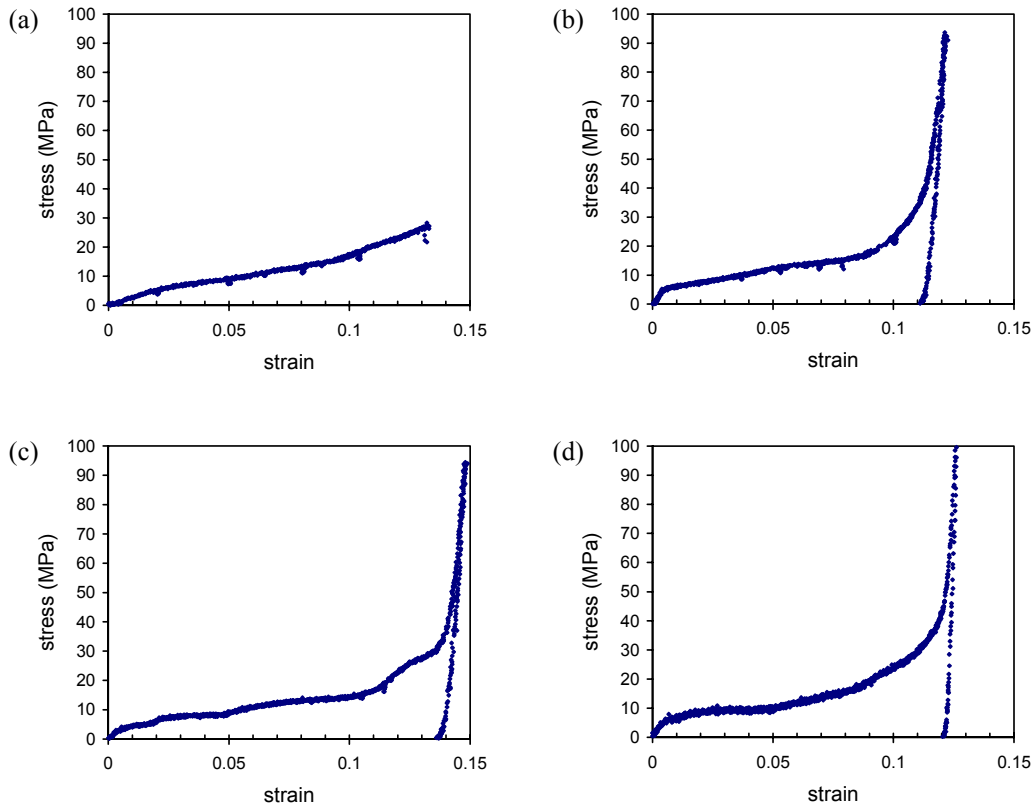


Figure 13. Stress–strain curves for a series of compression tests on sample 25-1-12 after applying magnetic field. (a) 1st compression along the 3 mm axis, (b) 2nd compression along the 6 mm axis, (c) 3rd compression along the 2.5 mm axis and (d) 4th compression along the 6 mm axis.

Figure 12a shows the 1st compression along the 6mm axis. The strain was about 5% and the twinning start stress was about 20 MPa. Moreover, dimension measurement conducted after the compression showed that both the 3mm and 2.5mm axes increased in length, although the percentage increase for the 3mm axis was about 3 times more than that of the 2.5mm axis. When compressed along the 3mm axis, the twinning start stress decreased to less than 10 MPa and the strain induced by twinning was more than

8% (Figure 12b), however, the test was programmed to unload before the twinning was completed. In this case, the length of the 2.5mm axis had a higher percentage increase than that of the 6mm axis. Figure 12c shows the result from the following compression along the 2.5mm axis. Similar to the previous case, the twinning start stress was about 10 MPa and the induced strain was more than 8%. The subsequent compression along the 6mm axis is shown in Figure 12d. The amount of induced strain was about 5% and the twinning start stress was less than 10 MPa, compared to about 20 MPa during the 1st compression. In addition, the stress did not linearly increase in the pseudo-elastic region, instead a significant change in slope can be observed. The reason for the change in slope is not clear. It is possible that multiple mechanisms for twin variants reorientation were involved. Further investigation is needed to clarify this.

After the last compression, a magnetic field of up to 1.1 T was applied along the 2.5mm, 3mm and 6mm axes in sequence. There was no detectable change in dimension after any of the three cases. When the magnetic field was applied along the 3mm axis, there was a strong tendency for the sample to rotate such that the 6mm axis was along the magnetic field direction. Compression tests were then conducted on the sample again after applying the magnetic field. Figure 13a shows the 1st compression along the 3mm axis. The strain induced by twinning was more than 13%. Moreover, a change in slope can be observed in the pseudo-elastic region. Figures 13b to 13d show the subsequent compression along the 6mm, 2.5mm and then the 6 mm axes, respectively. The twinning start stress was about 6 ~ 8 MPa and a twinning induced strain as high as 14% was observed.

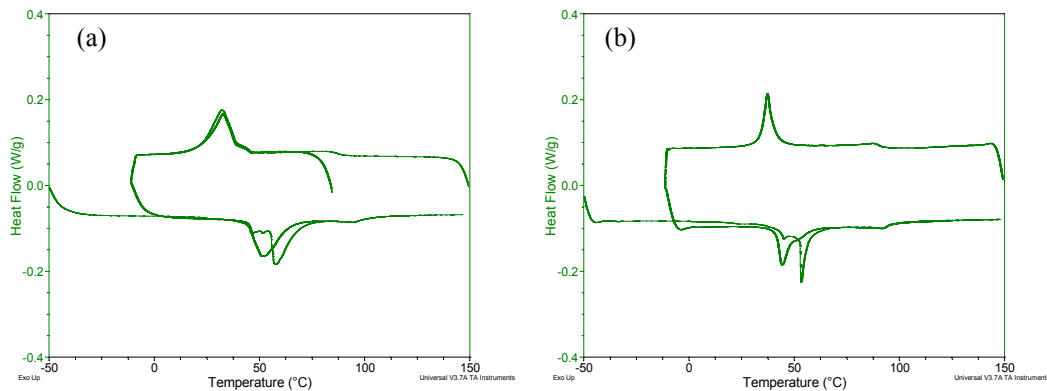


Figure 14. Differential Scanning Calorimeter curves for (a) sample 25-1-12 and (b) a small piece from sample 25-1-12 after compression tests.

Differential scanning calorimetry measurement was then carried out on the whole sample. The DSC cycling consisted of an initial cooling to -50°C, followed by a

controlled heating to 150°C and controlled cooling to -10°C, followed by two cycles of reheating to 90°C and cooling to -10°C. The DSC curve is shown in Figure 14a. Compared to Figure 14b, which is the DSC curve for a small piece cut out from sample 25-1-12 after all the compression tests have completed; the peaks in Figure 14a are much broader. Moreover, the peaks in Figure 14a are shifted to higher temperature during heating and lower temperature during cooling. These differences are believed [21] to be due to the size difference between the whole rectangular sample and the small piece (302 mg vs 17 mg). In addition, the austenite transformation temperature is higher during the first heating than those during the subsequent heating; it is believed that deformation of the sample may introduce residual stresses that suppress the transformation [22].

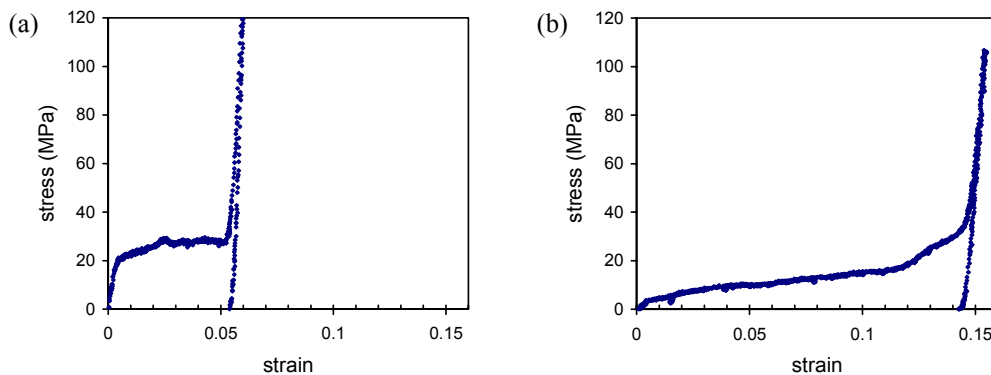


Figure 15. Stress–strain curves for a series of compression tests on sample 25-1-12 after DSC analysis: (a) 1st compression and (b) 3rd compression.

Compression tests were then conducted on the sample again after DSC analysis. Figure 15a shows the result from the 1st compression along the 6mm axis. The stress-strain curve is very similar to that right after heat treatment (Figure 12a). However, the starting stress decreased and the induced strain increased during the subsequent compression. Figure 15b shows the stress-strain curve for the 3rd compression, the starting stress was about 6 MPa and the strain was about 14%. This curve is almost the same as that in Figure 13c.

These results have shown that repeated applications of mechanical and magnetic forces can lower the twinning start stress and increase the twinning-induced strain. It is believed that the series of compression on the samples reduced the number of variants and increased the volume fraction of the major variants, and improved the mobility of the twin boundaries by unpinning the boundaries from pre-existing defects. The magnetization and magneto-mechanical measurements in this study suggested that Sample 25-1-9 has a 5M tetragonal martensitic structure. Moreover, heat treatments on this sample may improve the degree of ordering in the L2₁ Heusler phase [23,24],

which resulted in a larger twinning induced strain (up to 6%). Sozinov *et al.*[2] have shown that the alloy $\text{Ni}_{48.8}\text{Mn}_{29.7}\text{Ga}_{21.5}$ has a 7M orthorhombic crystal structure. Since the compositions of samples 25-1-14 and 27-8-1-13 (strain up to 8%) are very similar to this composition, it suggests that they also have a 7M orthorhombic structure, which is consistent with the magnetization measurement. However, no magnetic-field-induced strain was detected for sample 27-8-1-13. Moreover, sample 25-1-12, which also has a similar composition, showed up to 14% twinning strain. It is speculated that sample 25-1-12 may have a non-layered tetragonal structure. Thus, samples 25-1-14 and 27-8-1-13 may also have non-layered tetragonal structures and heat treatment improved the amount of twinning strain that can be obtained. On the other hand, it is possible that samples 25-1-14 and 27-8-1-13 have 7M orthorhombic crystal structures but the magnetic anisotropic energy is not sufficient to induce twin variants reorientation. The lowest twinning start and complete stresses for sample 27-8-1-13 were 6 MPa and 22 MPa, respectively. However, for the 7M orthorhombic $\text{Ni}_{48.8}\text{Mn}_{29.7}\text{Ga}_{21.5}$ alloy [2] that has a magnetic-field-induced strain of about 10%, the twinning start and complete stresses were only about 1 MPa and 2 MPa, respectively. In this case, the improved ordering of the austenite phase due to heat treatment may cause sample 25-1-12 to transform to non-layered tetragonal structure during transformation from austenite. The current study is still in progress, further work is required to clarify these questions. X-ray diffraction measurements are currently being carried out to determine the crystal structures and lattice parameters of these samples in order to calculate the theoretical maximum strain.

3.2 Effects of Temperature

Stress-strain curves from uniaxial compressions on sample 25-1-15 conducted at various temperatures are shown in Figure 16a. The rectangular sample was about 2mm×3mm×5mm in dimension. Before the measurements, repeated mechanical forces were applied to two orthogonal directions alternatively at room temperature to ensure a single-variant stage. At 23°C, the twinning start stress is less than 1 MPa with almost no increase in stress along the pseudo-elastic region. As shown in the figure, the twinning start stress increases with decreasing temperature. Twinning start stress is plotted as a function of the test temperature in Figure 16b. It seems that at temperatures slightly below M_F (31°C), the twinning start stress remains at almost constant. The twinning start stress increases substantially at temperatures more than 20°C below M_F ; and then it apparently reaches another plateau at lower temperatures. Moreover, the slope of the stress-strain curves along the pseudo-elastic region, which is the effective stiffness of the sample, also increases with decreasing temperature. This indicates that the dynamic resistance to twin boundary motion increases with decreasing temperature.

The effect of temperature on magnetic-field-induced strain is shown in Figure 17. To achieve a single-variant state prior to any strain measurement under magnetic field, the sample was first uniaxially compressed (up to 2 MPa) at 23°C in a direction orthogonal to that of the magnetic field and then unloaded [25]. The sample was then

cooled to the various test temperatures. At each test temperature, the applied magnetic field was then gradually increased to about 0.9 T. Decrease of temperature in the martensite affects notably the MSM behaviour. The curves in Figure 17 shift to the right with decreasing temperature. As shown in Figure 18a, the critical magnetic field required to initiate twin boundary motion increases with decreasing temperature. Moreover, the maximum observed magnetic-field-induced strain also decreases significantly with decreasing temperature (Figure 18b). Eventually, no measurable dimension change can be observed under magnetic field (up to 1.1 T) at temperatures below -11°C .

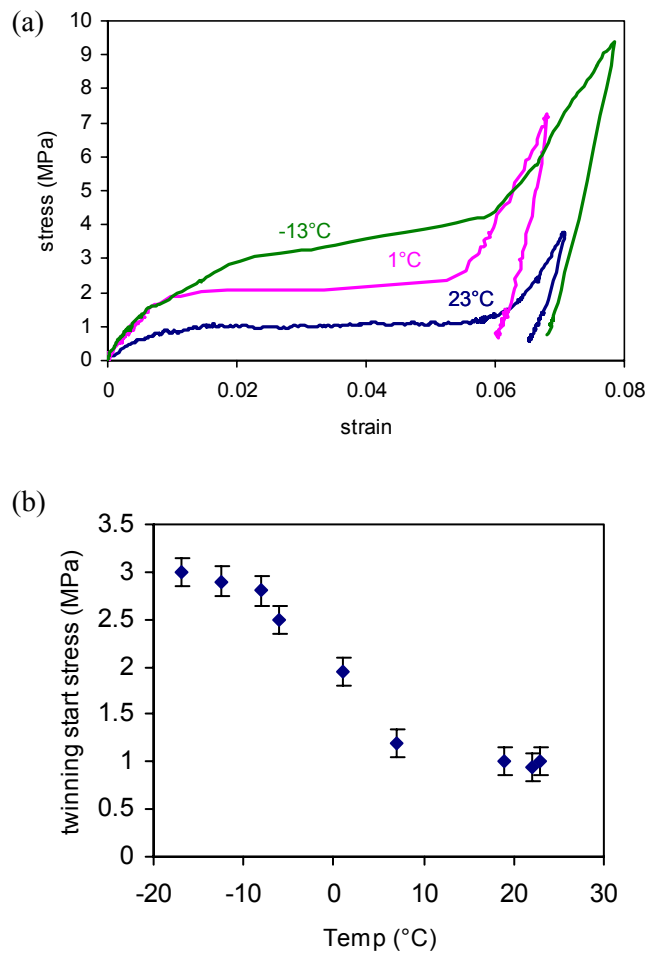


Figure 16. (a) Stress–strain curves and (b) twinning start stress of sample 25-1-15 during uniaxial compression as a function of temperature.

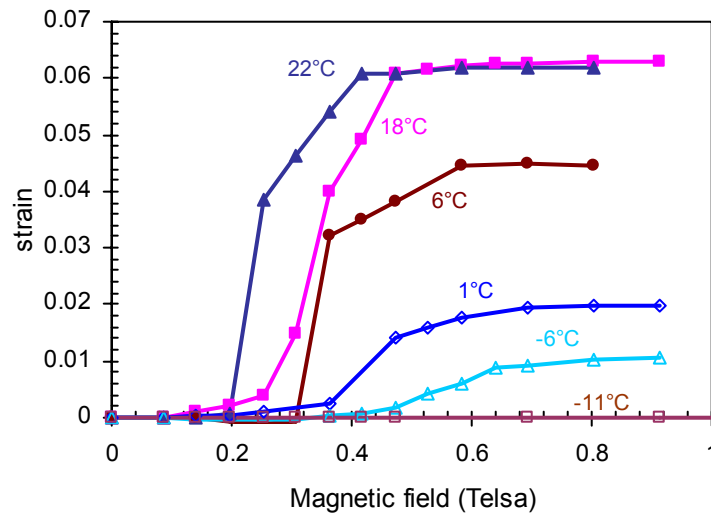


Figure 17. Effect of temperature on magnetic-field-induced strain in sample 25-1-15.

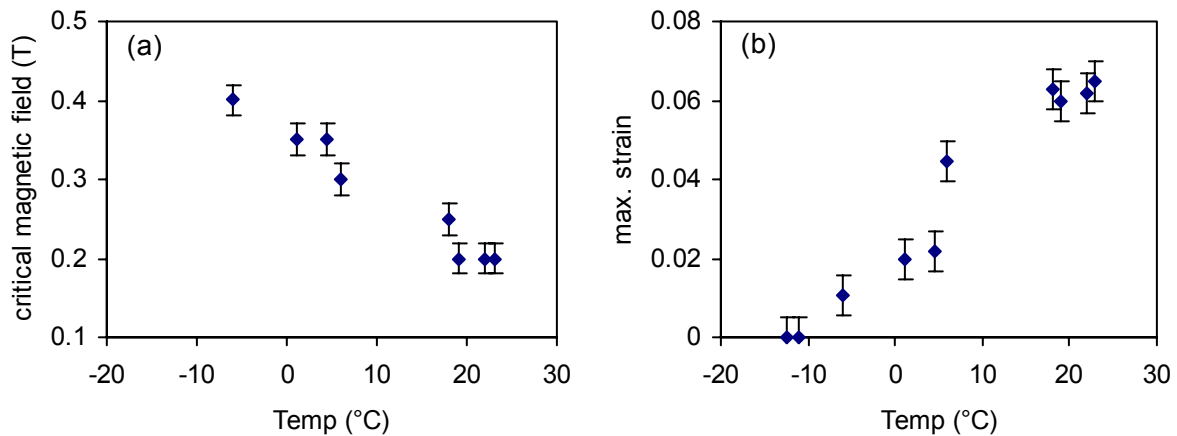


Figure 18. (a) Critical magnetic field and (b) maximum magnetic-field-induced strain as a function of temperature.

In addition, both the critical magnetic field and the maximum observed magnetic-field-induced strain remain almost constant at temperatures slightly lower than M_F , which are similar in trends to the temperature dependence of the twinning start stress. Glavatska *et al.* [26] have shown that for a Ni-Mn-Ga alloy with similar composition, the a - and c -cell parameters of the tetragonal cell only change slightly over a similar

temperature range. In fact, the c/a ratio increased about 0.34% with a 12°C decrease in temperature. Therefore, the change in lattice parameters and tetragonality does not account for the significant change in magnetic-field-induced strain with temperature change. Heczko *et al.* [27] have observed that the magnetic anisotropy constant in $\text{Ni}_{48.8}\text{Mn}_{28.6}\text{Ga}_{22.6}$ alloy increases from about $1.5 \times 10^5 \text{ J/m}^3$ at room temperature to about $2.0 \times 10^5 \text{ J/m}^3$ at 10°C. It is reasonable to expect similar change in magnetic anisotropy constant for the sample tested in the current investigation. Thus, it is proposed that the changes in MSM effect with temperature are mainly due to the changes in twinning start and finish stresses. Although the magnetic anisotropy increases with decreasing temperature, it is thought that it is not sufficient to overcome the increases in twinning start stress and twinning finish stress. As a result, higher applied magnetic field is required at lower temperature to initiate twin boundary motion. Moreover, with the increase in twinning finish stress at lower temperature, the equivalent stress induced by magnetic anisotropy is insufficient to complete the twinning motion. Therefore, the maximum observed magnetic-field-induced strain cannot reach the theoretical limit defined by the lattice parameters (i.e., $1-c/a$). Eventually, no MSM effect can be observed at sufficiently low temperature.

It is not clear whether similar strong temperature dependence can also be found in Ni-Mn-Ga alloys with different compositions and structures. Further investigation is being conducted to determine the relationship among temperature dependence, composition and structure. Temperature dependence of MSM effect in commercially available Ni-Mn-Ga will also be investigated.

4. Conclusions

Repeated mechanical and magnetic forces have been applied to Ni-Mn-Ga samples with different compositions and different thermo-magneto-mechanical histories in order to determine the combined effects of these parameters on the magnetic shape memory effects of these alloys. The results demonstrated that prior history could have strong influence on the twinning start stress and twinning strain. In addition, heat treatment of the materials seems to improve the ordering of the high temperature cubic phase that in turn increases the amount of strain that can be obtained (up to the theoretical limit). Moreover, there are indications that prior heat treatments may also affect the martensite crystal structure that is formed during cooling. However, further study is required to improve our understanding in these matters. Experiments are being carried out to determine the magnetic properties, crystal structure and lattice parameters of these alloys. Further investigation is also planned to study the effect of multiple deformation on the toughness and fatigue behaviour of the alloys.

Strong temperature dependence of the magnetic shape memory effect in a $\text{Ni}_{47.8}\text{Mn}_{27.5}\text{Ga}_{24.7}$ alloy has been observed. Although twinning start and finish stresses remain almost constant within about 20°C below M_F , they increase substantially at lower temperatures. Similar trends in temperature dependence have also been observed in critical magnetic field (increases with decreasing temperature) and the maximum magnetic field induced strain (decrease with decreasing temperature). Both parameters remain almost constant at temperatures slightly below M_F and then change significantly at lower temperatures. It is proposed that at lower temperatures the magnetic anisotropic energy is not sufficient to provide the driving force required for twin boundary motion. Thus, at lower temperatures, a higher magnetic field is required to induce twinning strain. The attainable magnetic-field-induced strains decrease with temperature until no magnetic shape memory effect can be observed at temperatures below -11°C. Further study is being conducted to investigate whether similar strong temperature dependence can also be observed in Ni-Mn-Ga alloys with different compositions and structures, including commercially available Ni-Mn-Ga alloys.

5. References

1. K. Ullakko, J.K. Huang, C. Kantner, V.V. Kokorin and R.C. O'Handley, "Large Magneto-mechanical properties and applications of Ni-Mn-Ga ferromagnetic shape memory alloy", *Applied Physics Letters*, 69, 1996, pp. 1966-1968.
2. A. Sozinov, A.A. Likhachev, N. Lanska, K. Ullakko and V.K. Lindroos, "Crystal structure, magnetic anisotropy and mechanical properties of seven-layered martensite in Ni-Mn-Ga", *Smart Structures and Materials 2002, Proceedings of SPIE*, Vol. 4699, 2002, pp. 195-205.
3. A. Sozinov, A. Likhachev, N. Lanska, and K. Ullakko, "Giant magnetic-field-induced strain in NiMnGa seven-layered martensitic phase", *Applied Physics Letters*, 80, 2002, pp. 1746-1748.
4. S.J. Murray, "Magneto-mechanical properties and applications of Ni-Mn-Ga ferromagnetic shape memory alloy", Ph.D. Thesis, MIT, Boston, MA, 2000.
5. S.-Y. Chu, R. Gallagher, M. De Graef and M.E. McHenry, "Structural and Magnetic Phase Transformations in Ni-Mn-Ga Ferromagnetic Shape-Memory Crystals", *IEEE Transactions on Magnetism*, 37, 2001, pp. 2666-2668.
6. R. Tickle, R. D. James, T. Shield, M. Wuttig, and V. V. Kokorin, "Ferromagnetic shape memory in the NiMnGa system", *IEEE Transactions on Magnetism*, 35, 1999, pp. 4301-4310.
7. S. J. Murray, M. Marioni, S. M. Allen, R. C. O'Handley, and T. A. Lograsso, "6% magnetic-field-induced strain by twin-boundary motion in ferromagnetic Ni-Mn-Ga", *Applied Physics Letters*, 77, 2000, pp. 886 - 888.
8. O. Heczko, A. Sozinov, and K. Ullakko, "Giant field-induced reversible strain in magnetic shape memory NiMnGa alloy", *IEEE Transactions on Magnetism*, 36, 2000, pp. 3266-3268.
9. A. Sozinov, Y. Ezer, G. Kimmel, P. Yakovenko, D. Giller, Y. Wolfus, Y. Yeshurun, K. Ullakko, and V. K. Lindroos, "Large magnetic-field induced strains in Ni-Mn-Ga alloy in rotating magnetic field", *J. Phys. IV (France)*, 11, 2001, pp. 311-316.
10. P. J. Webster, K. R. A. Ziebeck, S. L. Town and M. S. Peak, "Magnetic Order and Phase Transformation in Ni₂MnGa", *Phil. Mag. B*, 49, 1984, pp. 295-310.
11. J. Enkovaara, A. Ayuela, L. Nordström and R. M. Nieminen, "Magnetic anisotropy in Ni₂MnGa" *Phys Rev B*, 65, 134422, 2002, pp.1-7
12. V. V. Martynov, V. V. Kokorin, "The crystal structure of thermally- and stress-induced martensites in Ni₂MnGa single crystals", *J. Phys. III (France)*, 2, 1992, pp. 739-749.
13. A. Sozinov, A. A. Likhachev, and K. Ullakko, "Magnetic and magnetomechanical properties of Ni-Mn-Ga alloys with easy axis and easy plane of magnetization", *Proceedings of SPIE*, Vol. 4333, 2001, pp. 189-196.

14. A. Sozinov, A.A. Likhachev, N. Lanska, O. Söderberg, K. Ullakko and V.K. Lindroos, "Effect of crystal structure on magnetic-field-induced strain in Ni-Mn-Ga", *Proceedings of SPIE*, Vol. 5053, 2003, pp. 586-594.
15. J. Pons, V.A. Chernenko, R. Santamarta and E. Cesari, "Crystal structure of martensitic phases in Ni-Mn-Ga shape memory alloys", *Acta Mat.*, 48, 2000, pp. 3027-3038.
16. J. Chen, M. A. Gharghouri, and C. V. Hyatt, "Effects of Growth Rate and Composition on the Microstructure of Directionally Solidified NiMnGa Alloys", ed. D. C. Lagoudas, *Proceedings of SPIE*, Vol. 5053, 2003, pp. 181-190.
17. Nathan Benjamin and Leon M. Cheng, "Sample Preparation of Off-Stoichiometric Ni₂MnGa Ferromagnetic Shape Memory Alloys", DRDC Atlantic TN 2003-204, October 2003, 25 pages.
18. S.P. Farrell, R.A. Dunlap, C.V. Hyatt and L.M. Cheng, "Magnetic Properties of Ni-Mn-Ga Magnetic Shape Memory Alloys", *Proceedings of SPIE*, Vol. 5387, 2004, pp. 186-197.
19. Garrett Landry and Leon M Cheng, "Development of Magneto-Mechanical Actuator and Temperature Chamber for Characterization of Magnetic Shape Memory Alloys", DRDC Atlantic TN 2004-184, September 2004, 75 pages.
20. D.A. Filippov, V.V. Khovailo, V.V. Koledov, E.P. Krasnoperov, R.Z. Levitin, V.G. Shavrov and T. Takagi, "The Magnetic Field Influence on Magnetostructural phase transformation in Ni_{2.19}Mn_{0.81}Ga", *J. Magn. Magn. Mat.*, 258-9, 2003, pp. 507-509.
21. W.W. Wendlandt, *Thermal Analysis*, 3rd Edition, John Wiley & Sons, New York, 1986.
22. C.V. Hyatt, *et al.*, "Comparison of Martensite Transformation Temperatures in a NiMnGa Alloy Determined with Hot/Cold Stage Optical Microscopy and Differential Scanning Calorimetry", ed. D. C. Lagoudas, *Proceedings of SPIE*, Vol. 5053, 2003, pp. 576-585.
23. G.H. Wu, *et al.*, "Giant magnetic-field-induced strains in Heusler alloy NiMnGa with modified composition", *Applied Physics Letters*, 75, 19, 1999, pp. 2990-2992.
24. A.N. Vasil'ev, *et al.*, "Structural and Magnetic Phase Transitions in Shape-memory Alloys Ni_{2+x}Mn_{1-x}Ga", *Physical Review B*, 59, 1999, pp. 1113-1120
25. L.M. Cheng, S.P. Farrell, R. Ham-Su and C.V. Hyatt, "The Influence of composition and thermomechanical treatments on the magnetic shape memory effect of Ni-Mn-Ga single crystals", *Proceedings of SPIE*, Vol. 5387, 2004, pp.137-146.
26. N. Glavatska, G. Mogyl'ny, I. Glavatskiy, V. Gavriljuk, "Temperature stability of martensite and magnetic field induced strain in Ni-Mn-Ga", *Scripta Materialia*, 46, 2002, pp. 605-610.
27. O. Heczko, L. Straka, N. Lanska, K. Ullakko and J. Enkovaara, "Temperature dependence of magnetic anisotropy in Ni-Mn-Ga alloys exhibiting giant field-induced strain", *J. Applied Physics*, 91, 10, 2002 pp. 8228-8230.

Distribution list

Dr. Leon Cheng, DRDC Atlantic

Dr. Calvin Hyatt, DRDC Atlantic

Dr. Rosaura Ham-Su, DRDC Atlantic

Dr. Shannon Farrell, DRDC Atlantic

Dr. Richard Morchat, DRDC Atlantic

Library 6

DRDKIM 1

DOCUMENT CONTROL DATA		
(Security classification of title, body of abstract and indexing annotation must be entered when the overall document is classified)		
1. ORIGINATOR (the name and address of the organization preparing the document.. Organizations for whom the document was prepared, e.g. Centre sponsoring a contractor's report, or tasking agency, are entered in section 8.) DRDC Atlantic	2. SECURITY CLASSIFICATION (overall security classification of the document including special warning terms if applicable). UNCLASSIFIED	
3. TITLE (the complete document title as indicated on the title page. Its classification should be indicated by the appropriate abbreviation (S,C,R or U) in parentheses after the title). Magneto-Mechanical Response in Ni-Mn-Ga Magnetic Shape Memory Alloys		
4. AUTHORS (Last name, first name, middle initial. If military, show rank, e.g. Doe, Maj. John E.) Cheng, Leon M., Ham-Su, Rosaura, Farrell, Shannon P. and Hyatt, Calvin V.		
5. DATE OF PUBLICATION (month and year of publication of document) December 2004	6a. NO. OF PAGES (total containing information Include Annexes, Appendices, etc). 30 (approx.)	6b. NO. OF REFS (total cited in document) 26
7. DESCRIPTIVE NOTES (the category of the document, e.g. technical report, technical note or memorandum. If appropriate, enter the type of report, e.g. interim, progress, summary, annual or final. Give the inclusive dates when a specific reporting period is covered). Technical Memorandum		
8. SPONSORING ACTIVITY (the name of the department project office or laboratory sponsoring the research and development. Include address). Defence R&D Canada - Atlantic PO Box 1012 Dartmouth, NS, Canada B2Y 3Z7		
9a. PROJECT OR GRANT NO. (if appropriate, the applicable research and development project or grant number under which the document was written. Please specify whether project or grant). Project 11gm 13	9b. CONTRACT NO. (if appropriate, the applicable number under which the document was written).	
10a. ORIGINATOR'S DOCUMENT NUMBER (the official document number by which the document is identified by the originating activity. This number must be unique to this document.) DRDC Atlantic TM 2004-267	10b. OTHER DOCUMENT NOS. (Any other numbers which may be assigned this document either by the originator or by the sponsor.)	
11. DOCUMENT AVAILABILITY (any limitations on further dissemination of the document, other than those imposed by security classification) (X) Unlimited distribution () Defence departments and defence contractors; further distribution only as approved () Defence departments and Canadian defence contractors; further distribution only as approved () Government departments and agencies; further distribution only as approved () Defence departments; further distribution only as approved () Other (please specify):		
12. DOCUMENT ANNOUNCEMENT (any limitation to the bibliographic announcement of this document. This will normally correspond to the Document Availability (11). However, where further distribution (beyond the audience specified in (11) is possible, a wider announcement audience may be selected).		

13. **ABSTRACT** (a brief and factual summary of the document. It may also appear elsewhere in the body of the document itself. It is highly desirable that the abstract of classified documents be unclassified. Each paragraph of the abstract shall begin with an indication of the security classification of the information in the paragraph (unless the document itself is unclassified) represented as (S), (C), (R), or (U). It is not necessary to include here abstracts in both official languages unless the text is bilingual).

It is generally accepted that the large reversible, magnetic-field-induced strain observed in ferromagnetic shape memory alloys is due to the rearrangement of twin variants in the martensite by an applied magnetic field leading to an overall change of shape. The main thermodynamic driving force for twin boundary motion in the presence of a magnetic field is the high magnetocrystalline anisotropy of the low-symmetry martensitic phase. Low twin boundary energy, high magnetocrystalline anisotropy energy and saturation magnetization are some of the key factors for large magnetic field induced strain. In order to achieve optimum performance, thermomechanical and magnetic treatments are necessary. In this investigation, a systematic investigation is being carried out on single crystals of Ni-Mn-Ga alloys to determine the combined effects of composition and thermo-magneto-mechanical treatments on the crystal structure of the martensitic phases and the magneto-mechanical properties of the Ni-Mn-Ga alloys. Repeated mechanical and magnetic forces have been applied to the samples. The results demonstrate that prior history has strong influence on the twinning start stress and twinning strain. In addition, heat treatment of the materials seems to increase the amount of strain that can be obtained (e.g. increased from 3% to 6%). Moreover, there is indication that prior heat treatment may also affect the martensite crystal structure that is formed during cooling. A systematic investigation has also been carried out to determine the effect of temperature on the magneto-mechanical behaviour of the Ni-Mn-Ga alloys. Strong temperature dependence of the magnetic shape memory effect in a $\text{Ni}_{47.8}\text{Mn}_{27.5}\text{Ga}_{24.7}$ alloy has been observed. Twinning start and finish stresses, critical magnetic field and maximum magnetic-field-induced strain all remain almost constant within about 20°C below the martensite finish temperature and then change substantially at lower temperatures. Eventually no magnetic-field-induced strain can be observed at temperatures below -11°C. It is proposed that although magnetic anisotropy constant increases with decreasing temperature, it is not sufficient to overcome the increasing twinning stresses required for twin boundary motion at lower temperatures.

14. **KEYWORDS, DESCRIPTORS or IDENTIFIERS** (technically meaningful terms or short phrases that characterize a document and could be helpful in cataloguing the document. They should be selected so that no security classification is required. Identifiers, such as equipment model designation, trade name, military project code name, geographic location may also be included. If possible keywords should be selected from a published thesaurus. e.g. Thesaurus of Engineering and Scientific Terms (TEST) and that thesaurus-identified. If it not possible to select indexing terms which are Unclassified, the classification of each should be indicated as with the title).

Magnetic shape memory, Ni-Mn-Ga, magneto-mechanical, temperature dependence

This page intentionally left blank.

Defence R&D Canada

Canada's leader in defence
and National Security
Science and Technology

R & D pour la défense Canada

Chef de file au Canada en matière
de science et de technologie pour
la défense et la sécurité nationale



www.drdc-rddc.gc.ca